Magnetic Carbonyl Iron Suspension with Organoclay Additive and Its Magnetorheological Properties

Mpitloane Joseph Hato[1,2], Hyoung Jin Choi[2]*, Hyung Hoon Sim[2],

Byung Oh Park[2] and Suprakas Sinha Ray[1]

[1]*DST/CSIR Nanotechnology Innovation Centre, National Centre for Nano-Structured Materials, Council for Scientific and Industrial Research, P.O. Box395, Pretoria 0001*

Republic of South Africa

[2]*Department of Polymer Science and Engineering, Inha University, Incheon 402-751,*

Republic of Korea

---

* To whom correspondence should be addressed. E-mail: hjchoi@inha.ac.kr

Tel: +82-32-860-8777; Fax: +82-32-865-5178).

Abstract

Soft magnetic carbonyl iron (CI) based magnetorheological (MR) fluids containing three different loadings of submicron-sized organoclay were prepared. The MR characteristics were measured via rotational and oscillatory tests, in which the flow curves exhibited a non-Newtonian behavior for all investigated samples. The dynamic yield stress change was measured as a function of magnetic field strength by adopting a linear fit of the relation of log (τ_y) proportional to log (H), which was originally applied for electrorheological fluids. The viscoelastic performances of the pure CI suspension and the CI/organoclay suspensions showed the existence of a solid-like character. The sedimentation ratio was also investigated to confirm the role of sub-micron organoclay particles on the MR properties, in which the dispersion stability of pure CI was improved with increasing the content of organoclay in the CI suspension.

Key Words: Carbonyl iron; organoclay; magnetorheological fluid; sedimentation

1. Introduction

Magnetorheological (MR) fluids comprise of soft ferro-/ferri-magnetic particles suspended in nonmagnetic fluids such as hydrocarbon, silicone oil, or aqueous carrier fluid [1-6]. The MR fluids show the characteristic of Newtonian fluid when no magnetic fields are exerted. However, in the presence of magnetic field, they exhibit a continuous, rapid, and reversible change from a fluid-like state to a solid-like state within milliseconds [7, 8]. This is because dispersed magnetic particles can form chains which align in the direction of the magnetic field due to the magnetic-polarization interaction, and then returns to its free-flowing liquid state upon removal of the external magnetic field [9-11]. Due to their outstanding controllable mechanical characteristics, MR fluids have shown an immense interest from academia and industrial researchers to design a wide range of engineering applications such as shock absorbers, brakes, active dampers, and so on [12]. It is well known that during the dynamic phase transition, MR fluids transform to chain-like structures that lead to changes in rheological properties such as yield stress, shear viscosity, and the storage modulus similar to that of their electrorheological (ER) fluids counterparts [13-16]. A typical yield stress value which MR fluids can accomplish ranges from 10 ~ 100 kPa within possible magnetic field range. This value is in an order of magnitude higher than that of the ER fluids. Since magnetic fields are more stable in operation as compared to electric fields, a number of commercially available products of

MR fluids have been developed quite extensively than ER fluids [17].

Many kinds of magnetic species such as magnetite (Fe_3O_4), carbonyl iron (CI) and others have been investigated via diverse strategies to explore superior industrial demands of MR fluids [2, 18, 19]. Among all, a lot of studies have paid enormous attention on CI particles to fabricate MR fluids because of their fascinating magnetic properties, abundant availability as well as appropriate size [8, 20, 21]. However, its high density of about 7.86 g/cm^3 compared to the suspending medium oil, for instance, a lubricant oil of Yubase 8 (0.844 g/cm^3) induces serious sedimentation problem which result from large density mismatch between these two components. Based on this argument, CI particles create a major concern for being adopted in designing MR devices [22, 23]. Therefore, various researchers have introduced different techniques such as polymer coating on magnetic particles or introduction of additives such as thixotropic agents, surfactants, or fillers in order to overcome sedimentation problem. Among them, however, coating polymeric shells onto the surface of CI particles to reduce the density mismatch has been reported as a complex process in practice because of various factors affecting the coating thickness such as temperature, molar ratio among reactive agents or reaction time [20, 24, 25]. For this reason, introduction of additives into CI suspension has been reported as one prevailing method because they can prevent the physical contact of main magnetic particles, which can lead to hard baking [26, 27].

In recent years, several research groups have paid mammoth attention by using submicron-sized fillers such as polyhedral oligomeric silsequioxanes, clays and carbon nanotubes to prepare polymer composites because these materials possess excellent properties such as high surface areas as well as nano-scaled dimension [28-30]. When employing single-walled carbon nanotubes (SWNT) which intrinsically possesses some magnetic characteristics due to their residual iron catalyst resulting from synthesis process within the wall as an additive in the CI based MR fluid, a high yield stress with enhanced dispersion stability was observed. In addition, the viscoelastic behavior of the CI based MR fluid suggested a very strong solid-like characteristics [30].

In this paper, we report on the effect of different loadings of organically modified montmorillonite (OMMT) submicron-sized clay additive on carbonyl iron (CI) based MR fluid. Organoclay is used in this work because it can reduce particle settling and enhance flocculation stability of the MR based suspensions [27]. Rheological properties of the MR fluids under an applied magnetic field were studied via rotational and oscillatory tests. Sedimentation studies were also investigated.

2. Materials and methods

Soft magnetic carbonyl iron (CI, average particle size: 4.25 μm, density: 7.86 g/cm^3, BASF, Germany) particles and a lubricant Yubase oil (Yubase 8, dynamic viscosity: 46.48 cSt; density: 0.844 g/cm^3, SK Co., Korea) were used as a dispersed phase and suspending

medium for MR fluids, respectively. The OMMT used in this study was Cloisite 15A (commercially abbreviated as C15A), supplied by the Southern Clay Products, USA. We chose C15A due to its higher degree of hydrophobicity similar to that of lubricant oil as compared to other OMMTs. According to the supplier, the original clay Na^+-MMT was treated via a cation exchange reaction with a dimethyl, hydrogenated tallow (tallow consists of ~65 wt% C18, ~30 wt% C16, and ~5 wt% C14), 2-ethyhexyl, quaternary ammonium. The cation exchange capacity (CEC) of the MMT is 1.25 meq/g. To prepare the MR fluids, the concentration of CI was fixed to 25 wt% in all the systems and that of C15A was adjusted as 0.5, 1.0 and 3.0 wt% with respect to the suspending medium. The MR fluids were immersed in a sonifier for a few minutes to ascertain the required final homogeneity of the samples. In this work, the CI based MR suspensions containing 0.5, 1.0 and 3.0 wt% C15A loadings are abbreviated as CI/0.5 C15A, CI/1.0 C15A and CI/3.0 C15A suspensions, respectively. The MR characteristics were conducted using a rotational rheometer (MCR 300, Physica, Germany) connected to a magneto-rheological equipment (MRD 180, Physica, Germany) which generate a homogeneous magnetic field perpendicular to the shear flow direction. A 20 mm parallel-plate measuring system made up of nonmagnetic metal to prevent the occurrence of radial component of magnetic forces on the shaft of the measuring system at a gap distance of 1 mm was used. All the measurements were carried out at 26 °C. The sedimentation behaviour of pure CI and the

MR fluids was studied using Turbiscan (MA200, Turbiscan Laboratory, France).

3. Results and Discussion

The MR performances of various suspensions were conducted by using a rotational rheometer via a controlled shear rate (CSR) mode and the shear rate test ranging from 0.01 to 1000 s^{-1} via a log-log scale. To ensure reproducible results, suspensions were mechanically stirred using a vortex mixer for 2 min prior to MR characterization. Figures 1(a) – (c) present the flow characteristics of both pure CI and CI/C15A based MR fluids for different C15A loadings obtained in a controlled shear rate under varying external magnetic fields ranging from 0 to 342 kA/m of field strength. It is apparent that a typical observation of MR fluid was obtained, in which shear stress grows quickly under increased external magnetic field strength. The shear stress curves for pure CI and CI/C15A suspensions containing three different C15A loadings of 0.5, 1.0 and 3.0 wt% exhibit a non-Newtonian behaviour. This behavior is represented by showing a non-linear relationship between the shear stress and shear rate over the entire shear rate region studied. This behaviour can be attributed to an interparticle interaction, which indicates that the robust particle cluster structures constructed within fluid under an applied magnetic field are continuously broken and then reformed until the shear rate of 200 s^{-1} [23]. However, pure CI suspension and CI/C15A suspensions exhibit an opposite behavior at a very high shear rate region in the absence of external magnetic field, particularly in

the case of CI/3.0C15A suspension as shown in Fig. 1 (c)), in which the shear stress does not change very apparent which is similar with Newtonian fluid. This is a typical phenomenon observed in ER fluid which is analogous to MR fluid [31-33].

Fig. 1.

Figure 2 depicts the changes of shear viscosities for pure CI based MR suspension and different CI/C15A MR suspensions as a function of shear rate at four different magnetic field strengths of 0 to 342 kA/m. In order to control the properties of MR fluids, an increase in shear viscosity of the fluids plays a critical role. The induced magnetic moment of the particles caused by the exerted magnetic field is parallel to the direction of the field, while the viscocity of the flow is perpendicular to the magnetic field direction under the shear deformation. The resulting angle between magnetic moment and magnetic field gives rise to a magnetic torque hampering the free rotation of the particle and, hence, the shear viscosity of the fluid will increase [34]. From our results, it is also possible to observe an abrupt decrease of shear viscosity at a low shear rate region (shear thinning behaviour) for pure CI and CI/C15A MR suspensions, indicating that dispersed magnetic CI particle structures developed under external magnetic fields remained until the shear

rate of 200 s^{-1}. The shear thinning behavior is due to the changes of internal structures under shear deformation [23]. In addition, it is observable that in the absence of magnetic field strength the shear viscosity increases with increasing the loadings of C15A in the CI suspension as shown in Fig. 3, in which their rheological behaviors follow a conventional additive suspension system.

Fig. 2.

Fig. 3.

The oscillatory tests were carried out under four different magnetic field strengths of 0 to 342 kA/m in order to investigate the viscoelastic behaviour of the MR fluids when magnetic field is exerted. Parts (a) and (b) of Fig. 4 represent an amplitude sweep measurements which describe the changes of the storage modulus (G′) and loss modulus (G″) as a function of strain for CI based MR suspension and CI/3.0 C15A based MR suspension, in which both G′ and G″ designate the measurement of elasticity and viscous behavior of the fluid, respectively. The dynamic viscoelastic characteristics were determined using strain ranging from 0.001 to 100% and frequency ranging from 1 to 100 rad/s. It is obvious that G′ is considerably greater than G″ in the entire range of strain, which suggests the existence of a solid-like behavior than a liquid-like behavior. The G′

increases with increasing the magnetic field strengths for all the samples investigated.

Fig. 4.

Moreover, it is evident that at a fixed magnetic field strength, G′ values are independent of frequency, in which all samples exhibit plateau behavior over a wide range of frequency studied as shown in Fig. 5. This behavior indicates that the samples posses a very strong solid-like behavior rather than a liquid-like behavior [30, 35-37], which is an evidence of the dominating factor of elastic property over the viscous one. Furthermore, the CI/3.0 C15A MR suspension exhibits smaller G′ values as compared to both CI/0.5 C15A and CI/1.0C15A MR suspensions. This behavior could be due to the higher magnetic property of the CI particles as compared to the CI/OMMT systems. The increase in elastic performance is in accordance with the result of flow curves discussed above.

Fig. 5.

Our flow curves results indicated that both pure CI MR suspension and CI/C15A MR suspensions behave in a similar fashion, in which shear stress increases with magnetic field strength, which is a typical behaviour observed for ER fluids [30, 33]. Different

authors have suggested several models to describe the yield stress (τ_y) for both ER and MR fluids via shear stress equations [38-41].

By analyzing these models, our results indicate that the induced yield stress changes in a similar pattern, in spite of the applied external fields. The τ_y has been investigated as a function of the applied magnetic field strength (H_0) [42], in which the yield stress was divided into two different regimes based on H_0. At low H_0, τ_y is proportional to H^2, due to the local saturation of the magnetized particles, and typically approaches $H_0^{3/2}$ at higher H_0. It is known that for field strength high enough to achieve complete saturation, the particles can be treated rigorously as dipoles [42] and both the stress and modulus are independent of field strength and scale as saturation magnetization (M_S). In this case, under a moderate magnetic field strength, there may exist a critical magnetic field strength (H_c) satisfying $\tau_y \propto H_0^{3/2}$ ($H<H_c$) and $\tau_y \propto H_0^{2}$ ($H>H_c$). A universal yield stress equation was introduced by adopting critical electric field strength (E_c) to examine ER fluids indicated as follows [39]:

$$\tau_y(E_o) = \alpha E_o^2 \left(\frac{\tanh \sqrt{E_o/E_c}}{\sqrt{E_o/E_c}} \right) \quad (1)$$

where α is depended on various factors such as the dielectric constant of the fluid, the volume fraction of the particles as well as $\beta=(\varepsilon_p-\varepsilon_c)/(\varepsilon_p+2\varepsilon_c)$. ε_0 is permittivity of free space, ε_c is dielectric constant of liquid media, and ε_p is dielectric constant of solid

particles. E_c denotes the critical electric field strength originated from the nonlinear conductivity model and can be obtained as the crossover point of the slopes on E_0 *vs*. τ_y plot (in log-log scale).

Equation (1) has the following two limiting behavior at low and high electric fields represented by two regimes appeared in ER fluids [39], respectively:

$$\tau_y = \alpha E_o^{\,2} \quad , \qquad \text{for} \quad E_o << E_c , \tag{2a}$$

$$\tau_y = \alpha \sqrt{E_c} E_o^{\,3/2} \quad , \qquad \text{for} \quad E_o >> E_c . \tag{2b}$$

Equations (2) indicate that τ_y is proportional to E_0^2 (at a low electric field strength) and changes rapidly to $E_0^{3/2}$ for high E_0.

By normalizing Eq. (1) using E_c and $\tau_y(E_c) = 0.762\,\alpha E_c^{\,2}$ and

$$\hat{\tau} = 1.313\,\hat{E}^{3/2} \tanh\sqrt{\hat{E}} \tag{3}$$

Based on Eq. (3), yield stress data for ER fluids collapses onto a single curve for a wide range of electric field strengths.

Therefore, if we assume the similarity between ER and MR fluids, and hypothesize the existence of a H_c for MR fluids, a new universal yield stress correlation can be proposed as follows [30]:

$$\tau_y(H_o) = \alpha H_o^{\,2} \left(\frac{\tanh\sqrt{H_o/H_c}}{\sqrt{H_o/H_c}} \right) \tag{4}$$

Here, α is related to the susceptibility of the fluid and volume fraction or other

analogous physical parameters and τ_y have two limiting behaviors with respect to H_0,

$$\tau_y = \alpha H_o^{\,2} \qquad \text{for} \quad H_o << H_c, \tag{5a}$$

$$\tau_y = \alpha \sqrt{H_c} H_o^{\,3/2} \qquad \text{for} \quad H_o >> H_c. \tag{5b}$$

Fig. 6.

It is well known that the τ_y developed in the MR fluid increases monotonically with growing magnetic field strength. The τ_y continues to increase until the fluid reaches magnetic saturation. The dynamic yield stress as a function of magnetic field strengths for different CI/C15A suspensions is shown in Fig. 6. It can be seen that for both CI/0.5 C15A and CI/1.0 C15A suspensions, the dynamic yield stress accords very well with Eq. (4) and the H_c value is about 107.9 kA/m, while the magnitude of the slope, α for CI/3.0 C15A suspension, obtained from the linear relation τ_y *vs.* H^{α} (log-log scale) is 1.08 ± 0.005 [42]. However, it has been proposed that in the factual ER fluids, the value of α deviates from 2 due to several factors such as shape and concentration of the particle as well as nonlinear conductivity of the suspending medium oil [43-46]. A low value of α in the case of CI/3.0 C15A based MR system can be attributed to high concentration of C15A particles.

Then, a generalized scaling relationship can be obtained by scaling Eq. (4) via H_c and $\tau_y(H_c)=0.762\alpha\, H_c^{\,2}$ as:

$$\hat{\tau} = 1.313\,\hat{H}^{3/2}\tanh\sqrt{\hat{H}}\,. \qquad (6)$$

It is apparent that the data obtained from the flow curve, Fig. 1, collapses onto a single curve by employing Eq. (6) and the results are depicted in Fig. 7. It must be noted that in the case of CI/3.0 C15A based MR system, the data were chosen arbitrarily to obey Eq. (6). To improve the experimental data, a universal correlation in Eq. (6) can be modified by an additional parameter b, which was suggested for the systems that are not in good agreement with Eq. (6) while the plots seem to follow an alternative curve as reported by Choi *et al*. [39]. Therefore, we rescaled $\hat{\tau}$ with $\hat{\hat{\tau}} = \hat{\tau}\hat{H}^{4b}$ and $\hat{H}$ with $\hat{\hat{H}} = \hat{H}^{1+2b}$ and derived a modified scaling equation as follows:

$$\hat{\hat{\tau}} = 1.313\,\hat{\hat{H}}^{3/2}\tanh\sqrt{\hat{\hat{H}}} \qquad (7)$$

From Fig. 8, it can be seen that the points ($\hat{\hat{\tau}}$, $\hat{\hat{H}}$), which were recalculated by setting *b* = 0.29, were located along the curve of Eq. (7) with smaller deviations than the data ($\hat{\tau}$, $\hat{H}$) obtained using Eq. (6). For this reason, Eq. (7) can be useful in constructing the master curve for MR fluids. It is also notable that the deviation of the H_c does not change the scaled yield stress equation while the points obey the universal yield stress equation as reported elsewhere [41], increasing for higher H_c and goes down for lower H_c.

Fig. 7.

Fig. 8.

We also investigated the dispersion stability of the MR fluid by using Turbiscan. When sedimentation of particles takes place, the transmission profiles vary with the height of the cell with time and a transparent supernant forms because the magnetic particles sediment in suspending medium oil as shown in Fig. 9. The images on top are snapshots taken for CI and CI/C15A MR suspensions.

Fig. 9.

It is evident that the pure CI based MR suspension settles more faster than all that of CI/C15A based MR suspensions for the same duration of time due to density difference between pure CI and CI/C15A MR suspensions containing different C15A loadings, indicating that the dispersion stability of CI/C15A MR suspensions is better than that of pure CI. The improved dispersion stability is due to the gap-filling submicron-sized C15A particles between the micron-sized CI spheres. For this reason, the role of organoclay particles can be confirmed [27, 30].

4. Summary

This work presents the results on the preparation and characterization of MR fluids containing three different loadings of submicron-sized organoclay particles added in CI

suspension. The MR characteristics were found to be influenced by the presence of sub-micron organoclay particles. In addition, viscoelastic properties and the sedimentation were also investigated, in which a solid-like behavior was observed for all the samples while the presence of submicron-sized organoclay particles in the CI suspension exhibited an improved dispersion stability of the MR fluid.

Acknowledgement

This research was supported by the DST/CSIR, Republic of South Africa.

References

[1] A. J. Margida, K. D. Weiss, J. D. Carlson, Magnetorheological materials based on iron alloy, Int. J. Mod. Phys. B 10 (1996) 3335.

[2] B. O. Park, K. H. Song, B. J. Park, H. J. Choi, Miniemulsion fabricated Fe_3O_4/poly(methyl methacrylate) composite particles and their magnetorheological characteristics, J. Appl. Phys. 107 (2010) 09A506.

[3] O. E. Andrei, I. Bica, Some mechanisms concerning the electrical conductivity of magnetorheological suspensions in magnetic field, J. Ind. Eng. Chem. 15 (2009) 573.

[4] L. Tan, H. T. Pu, M. Jin, Z. H. Chang, D. C. Wan, J. L. Yin, Colloids Surf. A: Physicochem. Eng. Asp. 360 (2010) 137.

[5] H. An, S. J. Picken, E. Mendes, Enhanced hardening of soft-assembled copolymer gels under homogeneous magnetic fields, Soft Matter 6 (2010) 4497.

[6] B. J. Park, F. F. Fang, H. J. Choi, Magnetorheology: materials and application, Soft Matter 6 (2010) 5246.

[7] W. H. Li, H. Du, N. Q. Guo, Dynamic behaviour of MR suspensions at moderate flux densities, Mater. Sci. Eng. A 371 (2004) 9.

[8] X. Tang, X. Zhang, R. Tao, Y. Rong, Structure-enhanced yield stress of magnetorheological fluids, J. Appl. Phys. 87 (2000) 2634.

[9] H. B. Cheng, J. M. Wang, Q. J. Zhang, N. M. Werely, Preparation of composite

magnetic particles and aqueous magnetorheological fluids, Smart Mater. Struct. 18 (2009) 085009.

[10] S. Jenc, P. P. Phule, Rheological properties of magnetorheological fluids, Smart Mater. Struct. 11 (2002) 140.

[11] H. T. Pu, F. J. Jiang, Z. Yang, B. Yan, X. Liao, Effects of polyvinylpyrrolidone and carbon nanotubes on magnetorheological properties of iron-based magnetorheological fluids, J. Appl. Polym. Sci. 102 (2006) 1653.

[12] I. Bica, Electroconductive magnetorheological suspensions, Smart Mater. Struct. 15 (2006) N147.

[13] H. J. Choi, M. S. Jhon, Electrorheology of polymers and nanocomposites, Soft Matter 5 (2009) 1562.

[14] Q. Cheng, V. Pavlinek, Y. He, A. Lengalova, C. Li, P. Saha, Structural and eletrorheological properties of mesoporous silica modified with triethanolamine, Colloids Surf. A: Physicochem. Eng. Asp. 318 (2008) 169.

[15] P. Hiamtup, A. Sirivat, A. M. Jamieson, Hysteresis and strain hardening in the creep response of a polyaniline ER fluid, J. Colloid Interf. Sci. 325 (2008) 122.

[16] F. F. Fang, B. M. Lee, H. J. Choi, Electrorheologically intelligent polyaniline and its composites, Macromol. Research 18 (2010) 99.

[17] I. Bica, Damper with magnetorheological suspension, J. Magn. Magn. Mater. 241

(2002) 196.

[18] F. F. Fang, H. J. Choi, Fabrication of multiwalled carbon nanotube-wrapped magnetic carbonyl iron microspheres and their magnetorheology, Colloid Polym. Sci. 288 (2010) 79.

[19] A. J. F. Bombard, M. Knobel, M. R. Alcantara, Phosphate coating on the surface of carbonyl iron powder and its effect in magnetorheological suspensions, Int. J. Mod. Phys. B 21 (2007) 4858.

[20] I. B. Jang, H. B. Kim, J. Y. Lee, J. L. You, H. J. Choi, M.S. Jhon, Role of organic coating on carbonyl iron suspended particles in magnetorheological fluids, J. Appl. Phys. 97 (2005) 10Q912.

[21] J. De Vicente, M. T. López-López, J. D. G. Durán, F. González-Caballero, Shear flow behaviour of confined magnetorheological fluids at low magnetic field strengths, Rheol. Acta 44 (2004) 94.

[22] X. Z. Zhang, X. L. Gong, P. Q. Zhang, Q. M. Wang, Study on the mechanism of the squeeze-strengthen effect in magnetorheological fluids, J. Appl. Phys. 96 (2004) 2359.

[23] M. S. Cho, S. T. Lim, I. B. Jang, H. J. Choi, M. S. Jhon, Encapsulation of spherical iron- particle with PMMA and by its magnetorheological particles, IEEE Trans. Magn. 40 (2004) 3036.

[24] W. P. Wu, B. Y. Zhao, Q. Wu, L. S. Chen, K. A. Hu, The strengthening effect of guar

gum on the yield stress of magnetorheological fluid, Smart Mater. Struct. 15 (2006) N94.

[25] F. F. Fang, H. J. Choi, Noncovalent self-assembly of carbon nanotube wrapped carbonyl iron particles and their magnetorheology, J. Appl. Phys. 103 (2008) 07A301.

[26] E. Svasand, K. de Lange Kristiansen, O. G. Martinsen, G. Helgesen, S. Grimnes, A. T. Skjeltorp, Colloids Surf. A: Physicochem. Eng. Asp. 339 (2009) 211.

[27] S. T. Lim, H. J. Choi, M. S. Jhon, Magnetorheological characterization of carbonyl iron-organoclay suspensions, IEEE Trans. Magn. 41 (2005) 3745.

[28] M. J. Hato, S. Sinha Ray, A. S. Luyt, Nanocomposites based on polyethylene and polyhedral oligomeric silsesquioxanes, 1-microstructure, thermal and thermomechanical properties, Macromol. Mater. Eng. 293 (2008) 752.

[29] S. T. Lim, M.S. Cho, H.J. Choi, Magnetorheological characterization of organoclay added carbonyl-iron suspensions, Int. J. Mod. Phys. B 19 (2005) 1142.

[30] F. F. Fang, H. J. Choi, M. S. Jhon, Magnetorheology of soft magnetic carbonyl iron suspension with single-walled carbon nanotube additive and its yield stress scaling function, Colloids Surf. A: Physicochem. Eng. Aspects 351 (2009) 46.

[31] A. Chaudhuri, G. Wang, N. M. Wereley, V. Tasovksi, R. Radhakrishnan, Substitution of micron by nanometer scale powders in magnetorheological fluids, Int. J. Mod. Phys. B 19 (2005) 1374.

[32] Y. H. Cho, M. S. Cho, H. J. Choi, M. S. Jhon, Electrorheological characterization of

polyaniline-coated poly(methyl methacrylate) suspensions, Colloid Polym. Sci. 280 (2002) 1062.

[33] J. Claracq, J. Sarrazin, J.P. Montfort, Viscoelastic properties of magnetorheological fluids, Rheol. Acta 43 (2004) 38.

[34] K.V. Pfeil, M.D. Graham, D.J. Klingenberg, J.F. Morris, Structure evolution in electrorheological and magnetorheological suspensions from a continuum perspective, J. Appl. Phys. 93 (2003) 5769.

[35] K. H. Song, B. J. Park, H. J. Choi, Effect of nanoparticle additive on characteristics of magnetorheological fluid, IEEE Trans. Magn. 45 (2009) 4045.

[36] F. Jonsdottir, K. H. Gudmundsson, T. B. Dijkman, F. Thorsteinsson, O. Gutfleisch, Rheology of perfluorinated polyether-based MR fluids with nanoparticles, J. Intelligent Mater. Sys. Struct. 21 (2010) 1051.

[37] F. F. Fang, J. H. Kim, H. J. Choi, Synthesis of core-shell structured PS/Fe_3O_4 microbeads and their magnetorheology, Polymer 50 (2009) 2290.

[38] D. J. Klingenberg, F. van Swol, C. F. Zukoski, The small shear rate response of electrorheological suspensions I. Simulation in the point-dipole limit, J. Chem Phys 94 (1991) 6160.

[39] H.J. Choi, M.S. Cho, J.W. Kim, A yield stress scaling fucntion for electrorheological fluids, Appl. Phys. Lett. 78 (2001) 3806.

[40] P. Gonon, J. N. Foulc, P. Atten, C. Boissy, Particle–particle interactions in electrorheological fluids based on surface conducting particles, J. Appl. Phys. 86 (1999) 7160.

[41] Y. T. Choi, J. U. Cho, S. B. Choi, N. M. Wereley, Constitutive models of electrorheological and magnetorheological fluids using viscometers, Smart. Mater. Struct. 14 (2005) 1025.

[42] J. M. Ginder, L. C. Davis, L. D. Elie, Rheology of magnetorheological fluids: models and measurements, Int. J. Mod. Phys. B 10 (1996) 3293.

[43] J. W. Kim, S. G. Kim, H. J. Choi, M. S. Jhon, Synthesis and electrorheological properties of polyaniline-Na+-montmorillonite suspensions, Macromol. Rapid Commun. 20 (1999) 450.

[44] S. G. Kim, J. Y. Lim, J. H. Sung, H. J. Choi, Emulsion polymerized polyaniline synthesized with dodecylbenzene-sulfonic acid and its electrorheological characteristics: Temperature effect, Polymer 48 (2007) 6622.

[45] Q. Cheng, V. Pavlinek, Y. He, C. Li, P. Saha, Electrorheological characteristics of polyaniline/titanate composite nanotube suspensions, Colloid Polym. Sci. 287 (2009) 435.

[46] Y. D. Kim, D. De Kee, Measuring static yield stress of electrorheological fluids using the slotted plate device, Rheol. Acta 47 (2008) 105.

List of Figures

suspensions

Figure 7: Plot of $\hat{\tau}$ *vs.* $\hat{H}$ for three different CI/OMMT suspensions. Here, the data for CI/3.0 OMMT suspension were chosen arbitrarily to obey the universal equation. The solid line is obtained from Eq. (6).

Figure 8: Plot of $\hat{\hat{\tau}}$ *vs.* $\hat{\hat{H}}$ for various CI/OMMT suspensions. The solid line is obtained from Eq. (7)

Figure 9: Sedimentation ratio as a function of time for (a) pure CI suspension and CI/OMMT suspensions with different organoclay loadings of (b) 0.5 wt% (c) 1.0 wt% (d) 3.0 wt%.

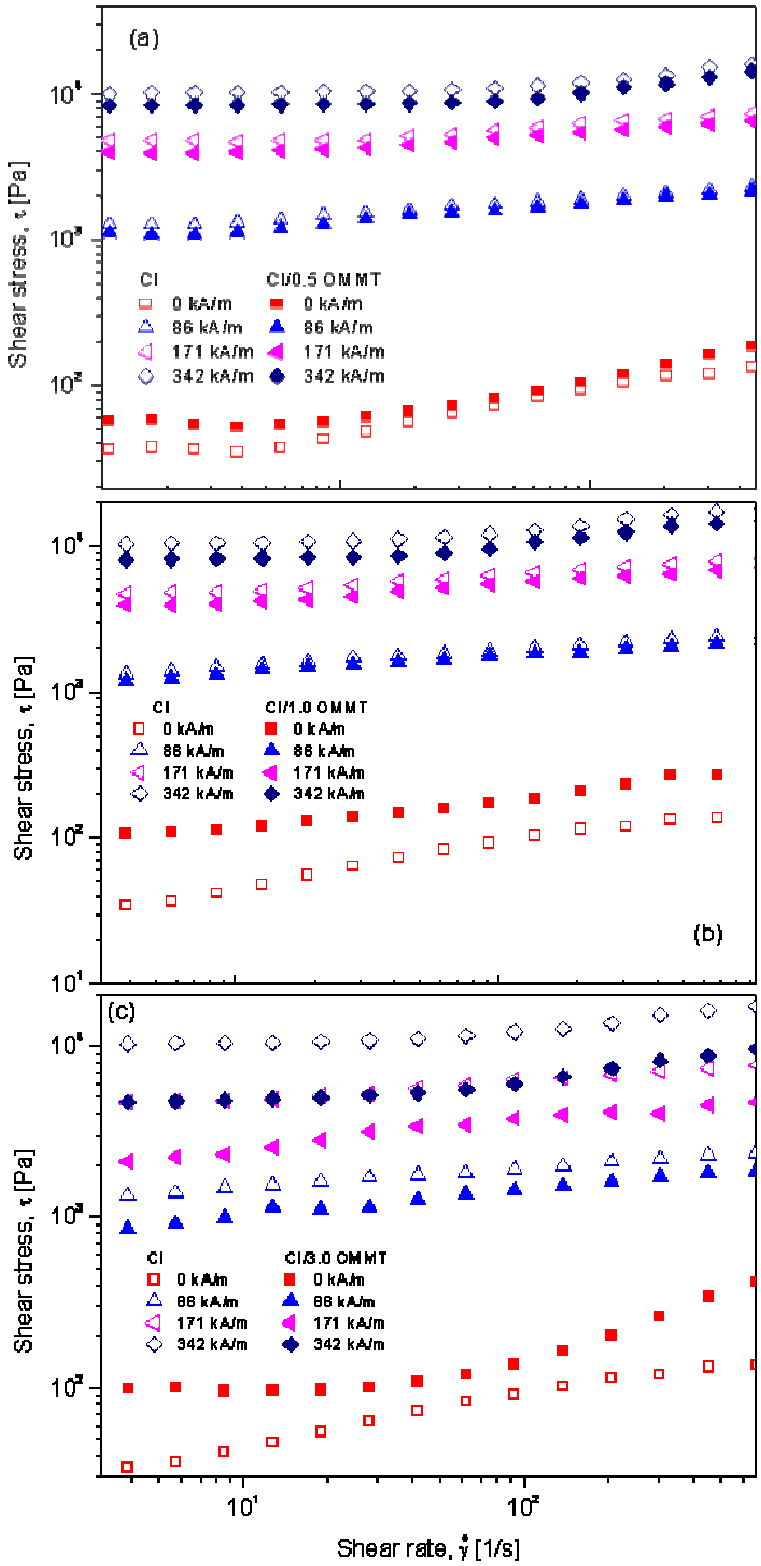
(a)
Shear stress, τ [Pa]
CI
0 kA/m
86 kA/m
171 kA/m
342 kA/m
CI/0.5 OMMT
0 kA/m
86 kA/m
171 kA/m
342 kA/m
(b)
CI/1.0 OMMT
(c)
CI/3.0 OMMT
Shear rate, γ̇ [1/s]

Fig. 1

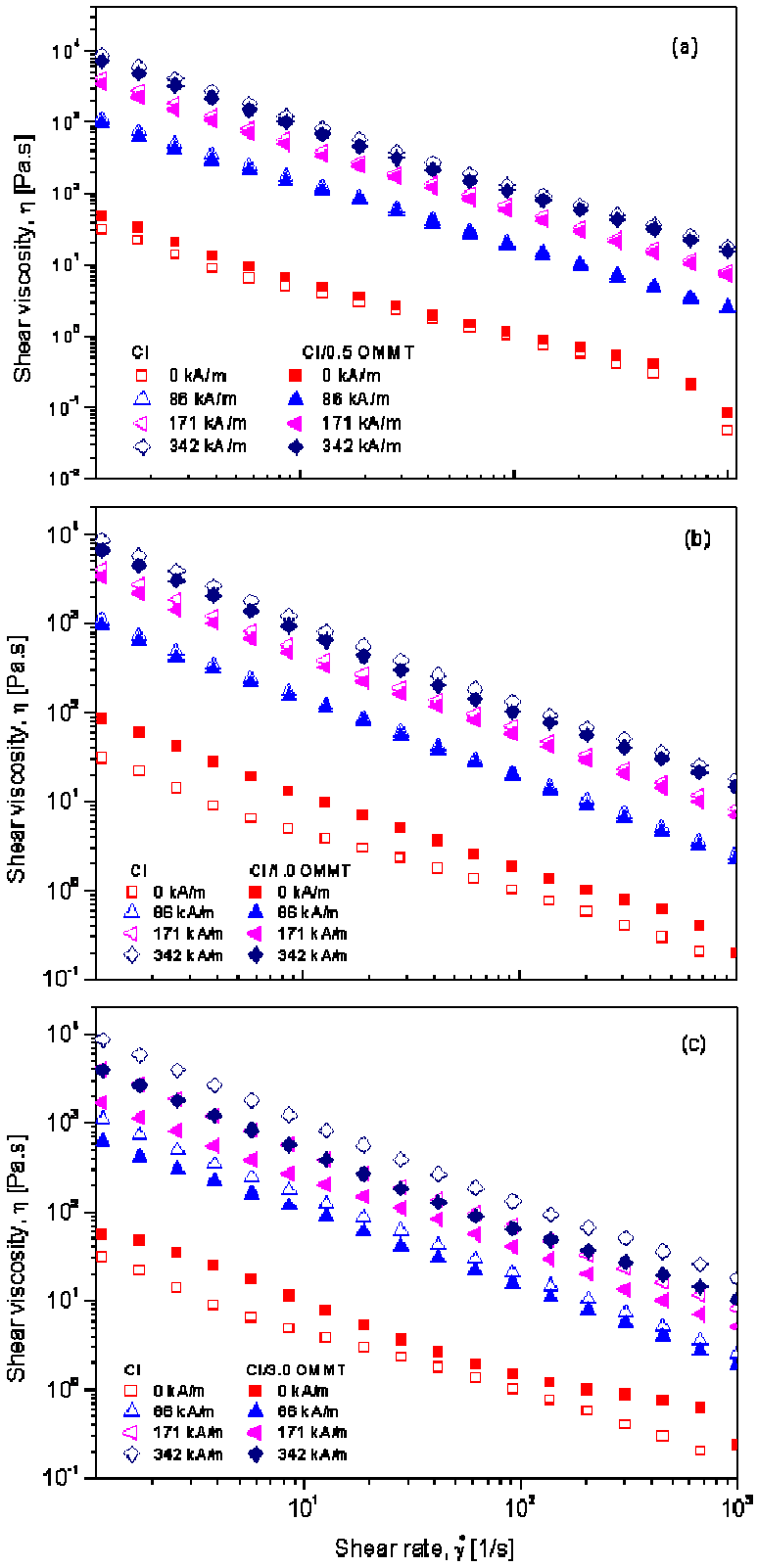
(a)
Shear viscosity, η [Pa.s]
CI
0 kA/m
86 kA/m
171 kA/m
342 kA/m
CI/0.5 OMMT
0 kA/m
86 kA/m
171 kA/m
342 kA/m
(b)
Shear viscosity, η [Pa.s]
CI
0 kA/m
86 kA/m
171 kA/m
342 kA/m
CI/1.0 OMMT
0 kA/m
86 kA/m
171 kA/m
342 kA/m
(c)
Shear viscosity, η [Pa.s]
CI
0 kA/m
86 kA/m
171 kA/m
342 kA/m
CI/3.0 OMMT
0 kA/m
86 kA/m
171 kA/m
342 kA/m
Shear rate, $\dot{\gamma}$ [1/s]

Fig. 2

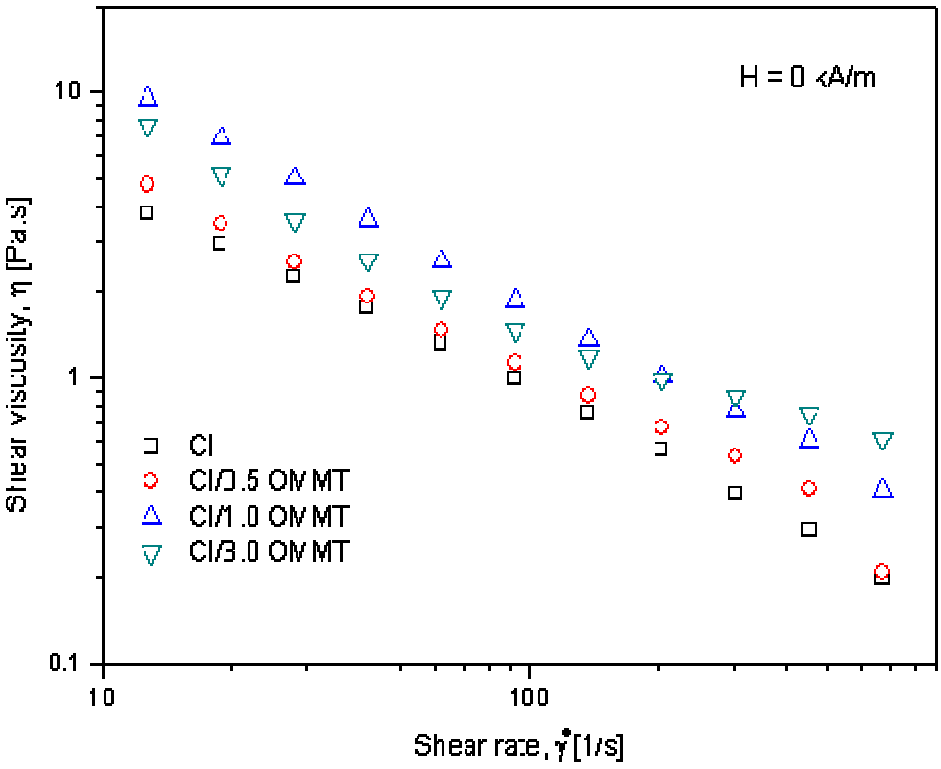
H = 0 kA/m
Shear viscusity, η [Pa.s]
Shear rate, γ̇ [1/s]
10
1
0.1
10
100
Cl
Cl/0.5 OMMT
Cl/1.0 OMMT
Cl/3.0 OMMT

Fig. 3

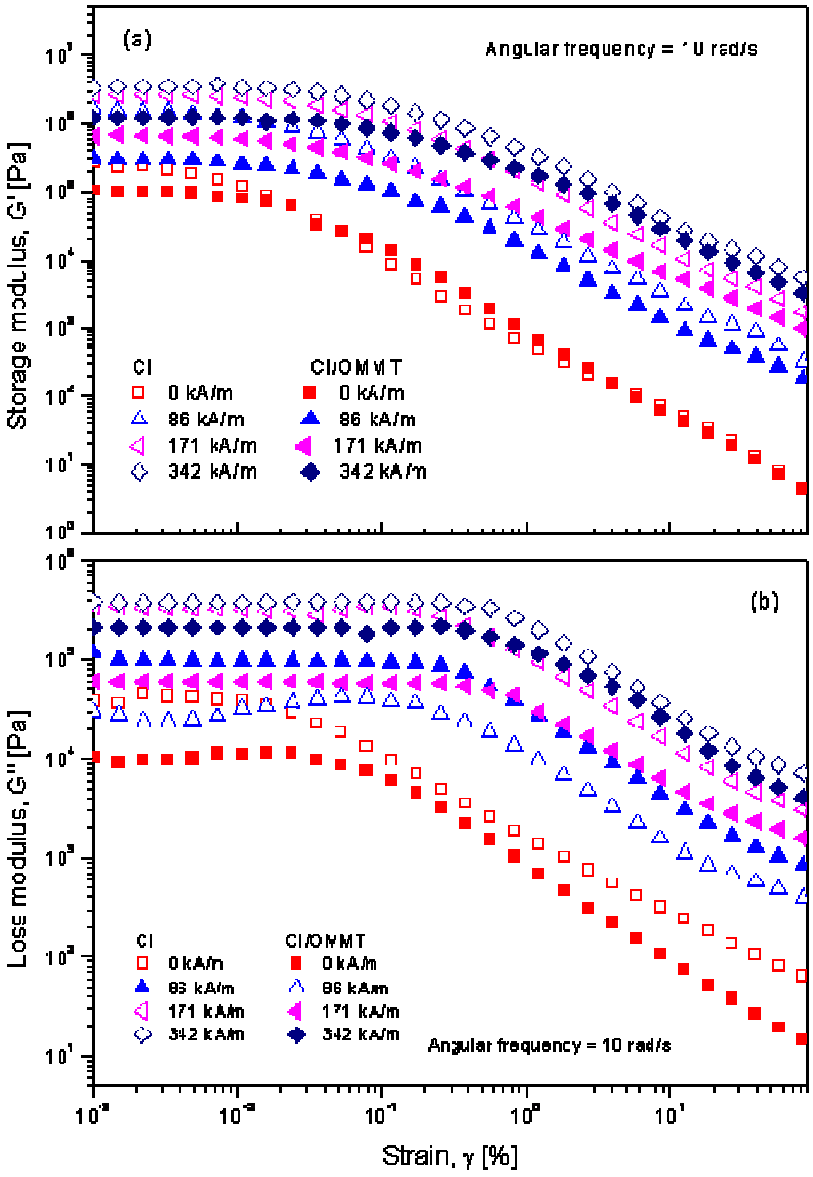
(a)
Angular frequency = 10 rad/s
Storage modulus, G' [Pa]
CI
0 kA/m
86 kA/m
171 kA/m
342 kA/m
CI/OMMT
0 kA/m
86 kA/m
171 kA/m
342 kA/m
(b)
Loss modulus, G'' [Pa]
Angular frequency = 10 rad/s
Strain, γ [%]

Fig. 4

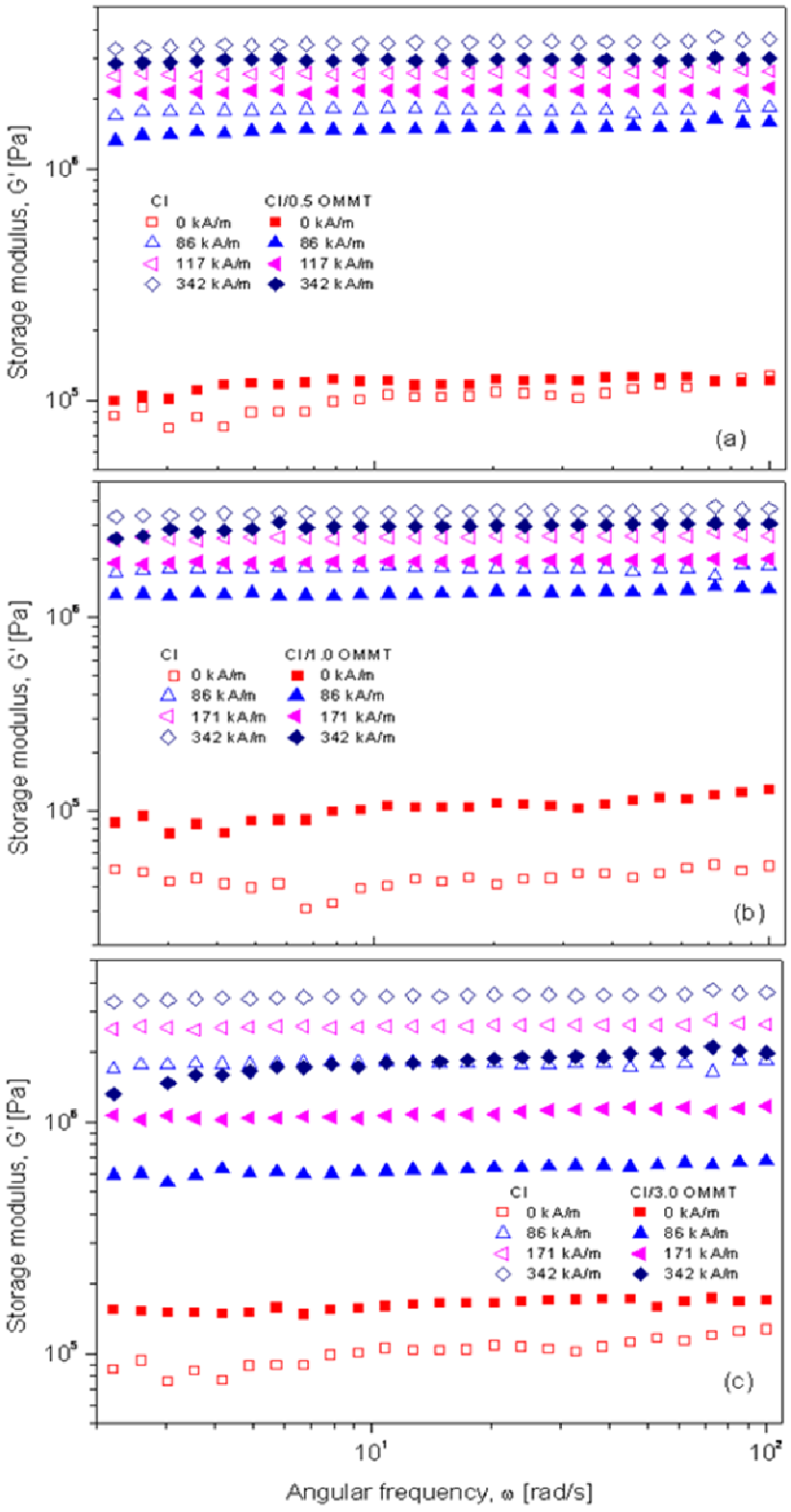
Storage modulus, G' [Pa]
10^6
10^5
CI
0 kA/m
86 kA/m
117 kA/m
342 kA/m
CI/0.5 OMMT
0 kA/m
86 kA/m
117 kA/m
342 kA/m
(a)
Storage modulus, G' [Pa]
10^6
10^5
CI
0 kA/m
86 kA/m
171 kA/m
342 kA/m
CI/1.0 OMMT
0 kA/m
86 kA/m
171 kA/m
342 kA/m
(b)
Storage modulus, G' [Pa]
10^6
10^5
CI
0 kA/m
86 kA/m
171 kA/m
342 kA/m
CI/3.0 OMMT
0 kA/m
86 kA/m
171 kA/m
342 kA/m
(c)
10^1
10^2
Angular frequency, ω [rad/s]

Fig. 5

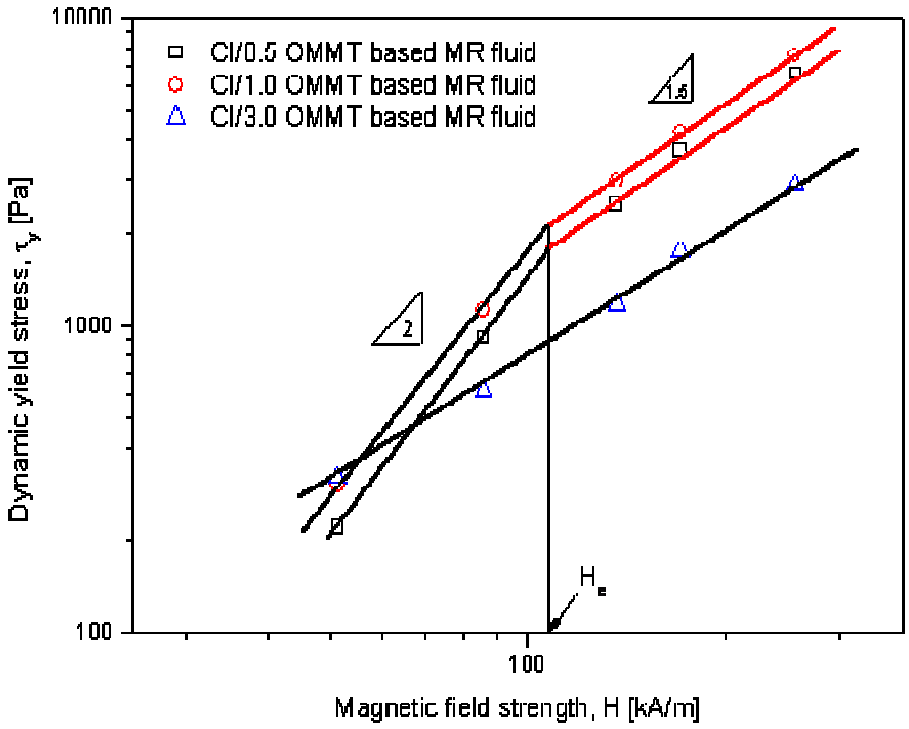
10000
1000
100
100
Dynamic yield stress, τ_y [Pa]
Magnetic field strength, H [kA/m]
Cl/0.5 OMMT based MR fluid
Cl/1.0 OMMT based MR fluid
Cl/3.0 OMMT based MR fluid
1.5
2
H_c

Fig. 6

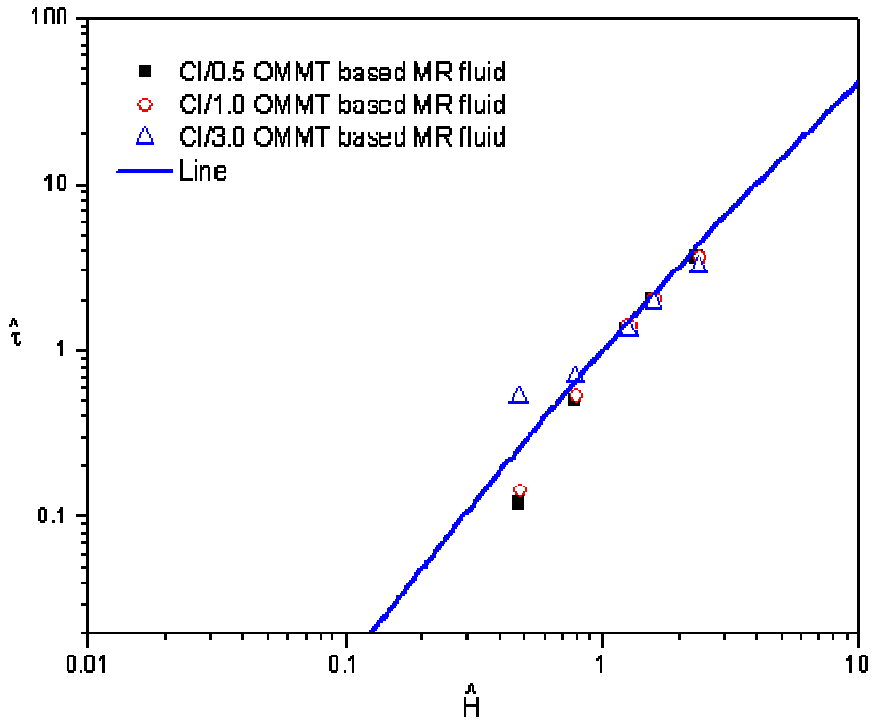
100
10
1
0.1
0.01
0.1
1
10
τ̂
Ĥ
CI/0.5 OMMT based MR fluid
CI/1.0 OMMT based MR fluid
CI/3.0 OMMT based MR fluid
Line

Fig. 7

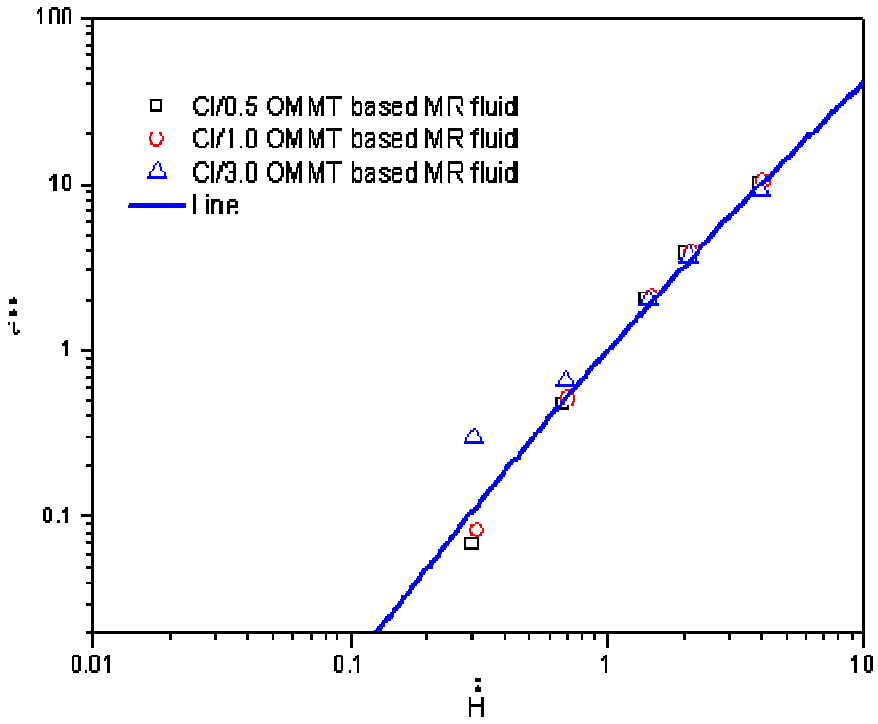
100
10
1
0.1
0.01
0.1
1
10
Cl/0.5 OMMT based MR fluid
Cl/1.0 OMMT based MR fluid
Cl/3.0 OMMT based MR fluid
Line

Fig. 8

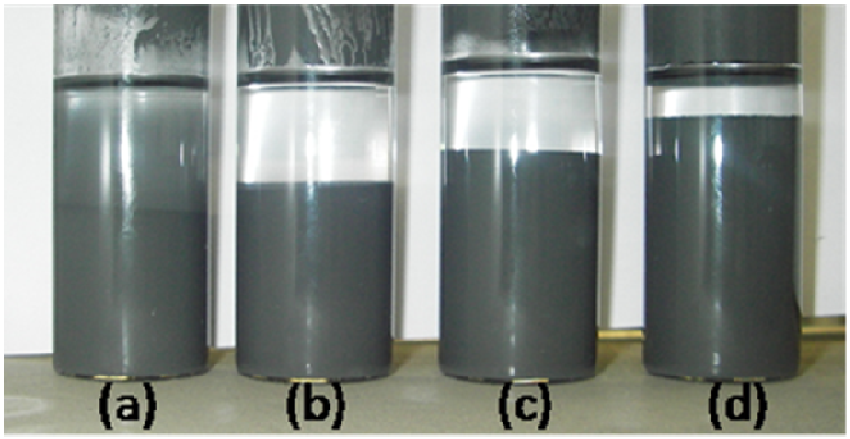
(a)
(b)
(c)
(d)

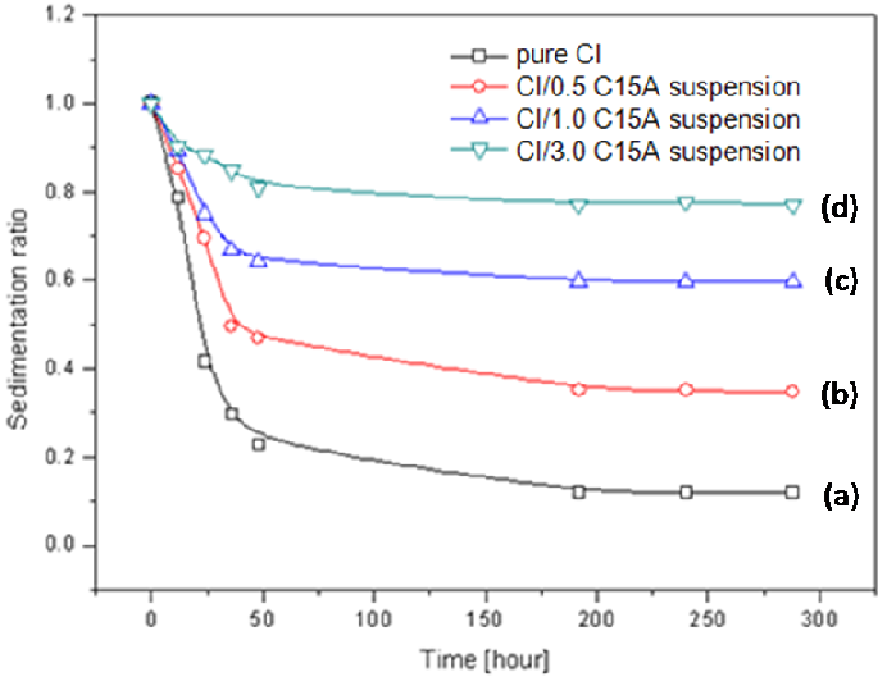
pure CI
CI/0.5 C15A suspension
CI/1.0 C15A suspension
CI/3.0 C15A suspension
(d)
(c)
(b)
(a)
Sedimentation ratio
Time [hour]
0.0
0.2
0.4
0.6
0.8
1.0
1.2
0
50
100
150
200
250
300

Fig. 9